The 2009 IEEE/RSJ International Conference on
Intelligent Robots and Systems
October 11-15, 2009 St. Louis, USA

Three Dimensional Statics for Continuum Robotics

Bryan A. Jones, *Member, IEEE*, Ricky L. Gray, and Krishna Turlapati, *Student Member, IEEE*

***Abstract*—This paper introduces a method for computing the shape of a continuously-flexible (continuum) robot in 3-D space which includes gravity loading by applying Cosserat rod theory to a continuum robot. With this theory, the shape of the rod can be determined using force-torque balance equations obtained from a simple free body diagram that represents the continuum robot. Real-time performance of 125 Hz makes this approach viable for the control of a continuum robot, enabled by avoiding boundary-value conditions in the solution.**

I. INTRODUCTION

Continuum robots, unlike traditional rigid-link robots, find their inspiration in the arm of an octopus, the trunk of an elephant, and the curl of the mammalian tongue. These biological structures, termed muscular hydrostats [1], rely entirely on soft, muscular tissue to grasp, manipulate, and explore a wide variety of objects. Similarly, continuum robots consist of a flexible structure whose shape is determined by all forces and moments experienced by the robot, in contrast to traditional rigid-link robots which exhibit large bending only at joints and whose shape can be determined by kinematics. Like an elephant trunk, these robots can perform whole-arm grasping [2] to grasp and manipulate objects over a wide range of sizes [3]. Like the mammalian tongue, they curl and stretch to deliver sensors to hard-to-reach areas [4]. Just as octopi use their arms to strike with amazing speeds in order to catch their prey [5], so continuum trunks can perform open-loop grasping [3].

This wide variety of abilities results in a number of unique applications for continuum robots. In the medical field, applications include use as active cannulas [6, 7], endoscopes [8], colonoscopes [9], in minimally-invasive surgery [10], and much more. They also find use in hot-cell decontamination [11, 12], undersea manipulation [13, 14], and disaster relief [15].

However, despite a number of prototypes constructed [16], models which ignore the non-linear effects of gravity loading produce significant errors when calculating a continuum robot's shape. This makes shaping these robots to perform useful tasks difficult with the current methodology, while models which incorporate gravity loading have not been applied to real-time control because these more accurate models require a significant amount of time to compute trunk position [17]. This paper seeks to close this gap by applying modeling techniques which account for all forces and moments applied, such as gravity-induced sag, yet retain the efficiency to be applied to real-time control of a continuum robot.

II. BACKGROUND AND RELATED WORK

A model which predicts the shape of a continuum robot with high accuracy enables fine control of that robot's shape. The difficulty in determining this model and in computing it in real-time, in order to shape a continuum robot, leads to several approaches.

One widely-adopted approach [6-9, 18, 19] simplifies the problem by neglecting the effects of gravity in determining the shape of the continuum robot, yielding shapes composed of piecewise circular arcs. The resulting analytical solutions produce excellent real-time performance at the expense of accuracy. Experiments with continuum robots whose shape is calculated based on this approach demonstrate significant errors in predicted verses actual trunk tip location [17, 20].

Pioneering work investigating the locomotion of snakes [21] developed two curves (clothoid and serpenoid) which approximates the shape of a snake's 2-D trajectory. While helpful, it does not provide a method for modeling the shape of a continuum trunk, which differs significantly in mechanical construction when compared to a snake. A second method [22] involves first choosing a curve with convenient mathematical properties, then fitting a robot to that curve. However, the difficulty of performing this matching for a continuum robot equipped with a finite number of actuators and constrained by sag due to gravity results in few applications of this method.

A third choice involves modeling a continuum robot as a curve in space shaped by shear, extension, and bending. An orientation assigned to each point along this curve gives the

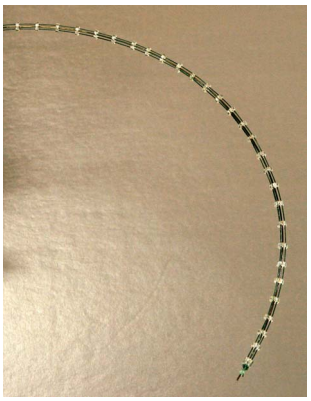

Fig. 1 Prototype continuum robot. The approach described in this paper should describe its shape.

Bryan A. Jones is with the Department of Electrical and Computer Engineering, Mississippi State University, Mississippi State, MS 39762 USA (phone: 662-325-3149; fax: 662-325-9438; e-mail: bjones @ ece.msstate.edu).

Ricky L. Gray is with the Department of Electrical and Computer Engineering, Mississippi State University, Mississippi State, MS 39762 USA (phone: 662-418-0307; fax: 662-325-9438; e-mail: rlg50@msstate.edu).

Krishna Turlapati is with the Department of Electrical and Computer Engineering, Mississippi State University, Mississippi State, MS 39762 USA (phone: 845-544-0746; fax: 662-325-9438; e-mail: kvt11 @ msstate.edu).

plane in which the cross-section of the rod lies. This formulation is termed a special Cosserat rod. While a continuum robot is not physically composed of a set of infinitesimally small points in space which comprise a curve, the slenderness of the robot compared to its length suggests this as a reasonable approximation, which is experimentally validated later in this paper. More detailed models which track the location of each point composing the rod exist; however, the increased accuracy of these models is unlikely to justify the higher computational effort required to use them. Rather, this paper builds upon the theory of Cosserat rods which has been refined through centuries of development by eminent mathematicians and physicists and is successfully applied in the fields of mechanical, civil, and structural engineering.

In particular, as described in [23], James Bernoulli began in the late 1700s the development of a theory which describes the bending of a rod in two dimensions under the influence of forces and moments. Later work by Euler and Daniel Bernoulli led to their classical theory of rod deformation in 2-D. Contributions by Kirchhoff, Love, and others led development of the theory to 3-D, which the Cosserats generalized in the early 19th century. Shear forces incorporated by Timoshenko and contributions by many others led to its present form in Antman's seminal work.

All works which apply rod theory to continuum robots likewise define a continuum robot as a series of points and associated orientations which define a curve in space, though not all make use of special Cosserat rods. Specifically, a series of papers by Ivanescu (see e.g. [24]) derive the dynamics of linear, elastic rods in 3-D based on an energy-work relationship developed by the author, which then provide the basis for various control techniques applied to the trunk. In contrast, work in [25] utilized variational methods for Cosserat rods founded in classical mechanics developed by Love to determine the dynamics of linear, elastic rods in 2-D actuated by cables, then uses this formulation to prove the stability of an associated control system. Finally, [17] applies Antman's work in Cosserat rods [23] to a continuum trunk in 3-D, which provides significantly improved agreement with a physical trunk when compared to simpler models.

However, no attempt was made to apply these results to control a robot, or investigate real-time performance. This paper presents the development of this theory in a form amenable to real-time control of a multi-section continuum robot in 3-D through analysis of the statics of rod deformation.

III. Statics of Rod Deformation in 3-D

Defining the shape of a rod and therefore the shape of a continuum robot requires consideration of three topics. First, rod kinematics provide a general method for defining a space curve with an associated orientation. Next, a section on mechanics presents a force and moment balance, which provides an opportunity to include the deformation due to gravity in the equations. Finally, constitutive equations relate forces and moments to kinematic displacements, while initial and boundary conditions provide information necessary to complete the solution of the problem.

A. Kinematics

A special Cosserat rod is parameterized by its reference, unstretched length by the variable s as shown in Fig. 2(b). Choosing the three-element vector $\mathbf{r}(s) \in \mathbb{R}^3$ to specify the location of a point on the rod, $\mathbf{r}(0\text{ cm})$ gives the rod's location at its origin while $\mathbf{r}(40\text{ cm})$ gives the location of a point 40 cm from the origin, measured before the rod's length changes due to stretching or compression. In addition, a rotation matrix $\mathbf{R}(s) \in SO(3)$ specifies the orientation of the rod with respect to a global coordinate frame by establishing a local coordinate frame attached to the rod at $\mathbf{r}(s)$. Therefore, for any vector $\mathbf{a}$, $\mathbf{a} = \mathbf{R}\mathbf{a}^l$ and $\mathbf{a}^l = \mathbf{R}^{\mathrm{T}}\mathbf{a}$ provides transformation between local and global frames. The appearance of the superscript l indicates specification in local coordinates; vectors or matrices with no superscript remain in the global frame. Finally, recording only local changes in translation $\mathbf{v}^l(s)$ and changes in orientation $\mathbf{u}^l(s)$ for an infinitesimally small section of the rod significantly simplifies the problem by postponing knowledge of overall, global rod shape until a final integration step.

Physically, the spatial velocity vector $\mathbf{v}^l = \begin{bmatrix} v_1^l & v_2^l & v_3^l \end{bmatrix}^{\mathrm{T}}$ as shown in Fig. 2(c) specifies shear along the local x and y axes in $v_{1\ldots2}^l$ and rod stretch or compression in v_3^l, where $v_3^l = 1$ denotes neither stretch nor compression, $0 < v_3^l < 1$ compression (note the case $v_3^l = 0$ of infinite compression is not allowed), and $v_3^l > 1$ stretch. Likewise, the spatial angular velocity vector $\mathbf{u}^l = \begin{bmatrix} u_1^l & u_2^l & u_3^l \end{bmatrix}^{\mathrm{T}}$ pictured in Fig. 2(a) specifies bending of the rod, where positive values indicate bend in a counterclockwise direction. Specifically, $u_{1\ldots2}^l$ specifies bending about the local x and y axes. By convention, the rod extends along the local z axis, so u_3^l gives twist about the rod.

This linear velocity causes changes to the rod's position of $\dot{\mathbf{r}}^l(s) = \mathbf{v}^l(s)$, where a dot indicates derivatives according to s. In the global frame,

$$\dot{\mathbf{r}}(s) = \mathbf{R}(s)\,\mathbf{v}^l(s). \tag{1}$$

Likewise, angular velocity causes changes to the orientation of the rod of $\dot{\mathbf{R}}(s) = \hat{\mathbf{u}}(s)\mathbf{R}(s)$ where the hat indicates placing an angular velocity vector into a skew-symmetric matrix. Transforming to local coordinates for bending,

$$\dot{\mathbf{R}}(s) = \mathbf{R}(s)\,\hat{\mathbf{u}}^l(s). \tag{2}$$

B. Mechanics

A free-body diagram provides both force and moment (torque) balance equations. The force balance precedes the moment balance, since an essential substitution in the moment balance requires reference to results from the force balance.

1) Force balance

Consider a segment of the rod from point c to a point s on the rod illustrated in Fig. 3. Internal rod forces due to stretching and shearing the rod, termed contact forces, are $\mathbf{n}(s) - \mathbf{n}(c)$, where $\mathbf{n}(s) \in \mathbb{R}^3$ specifies the force applied to

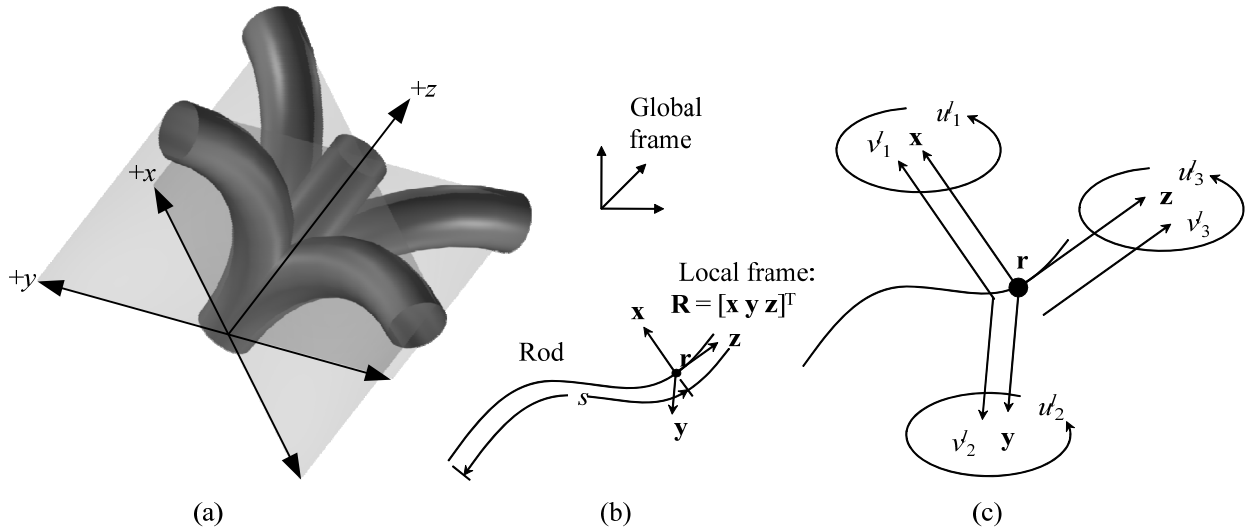

Fig. 2 In (a), a graphical definition of **u**, with local axes shown. A rod may bend about the local *x* or *y* axis or twist about the local *z* axis. Illustration (b) shows that a rod consists of a position $\mathbf{r}(s)$ and orientation $\mathbf{R}(s)$ defined at every point along the rod. Definition of $\mathbf{R}(s)$ creates a local coordinate frame at each point on the rod. In (c), shear strains $\mathbf{v}^l$ and bending strains $\mathbf{u}^l$ referenced to this coordinate system shape the rod.

this segment by the distal section of the rod (from *s* to the rod's tip) while $-\mathbf{n}(c)$ gives the force applied to this segment by the proximal section of the rod (from the beginning of the rod to *c*). All other forces are termed body forces; gravity loading is one such force. Assuming these body forces applied at some point *a* on the rod are captured in $\mathbf{f}(a)$, then summing these forces over all points in the segment gives a total force of $\int_c^s \mathbf{f}(\xi)\,d\xi$. Therefore, the overall balance is

$$\mathbf{n}(s)-\mathbf{n}(c)+\int_c^s \mathbf{f}(\xi)\,d\xi=\mathbf{0}. \tag{3}$$

Computing the partial derivative of with respect to *s*,

$$\dot{\mathbf{n}}(s)+\mathbf{f}(s)=\mathbf{0}. \tag{4}$$

2) Moment balance

The moment balance incorporates the effects of all forces applied at a distance and of applied moments (torques). Like the force balance, one moment results from bending of the rod $\mathbf{m}(s)-\mathbf{m}(c)$. Forces in the rod applied at a distance produce the moment $\mathbf{r}(s)\times\mathbf{n}(s)-\mathbf{r}(c)\times\mathbf{n}(c)$. Body couples (analogous to body forces **f**, but for moments) are $\int_c^s \mathbf{l}(\xi)\,d\xi$, and moments due to body forces applied at a distance produce $\int_c^s \mathbf{r}(\xi)\times\mathbf{f}(\xi)\,d\xi$. Collecting terms produces $\mathbf{m}(s)-\mathbf{m}(c)+\mathbf{r}(s)\times\mathbf{n}(s)-\mathbf{r}(c)\times\mathbf{n}(c)+\int_c^s\left(\mathbf{r}(\xi)\times\mathbf{f}(\xi)+\mathbf{l}(\xi)\right)d\xi$. Taking a partial derivative according to *s* then substituting (4) and noting that these terms must balance by summing to zero, $\dot{\mathbf{m}}(s)+\dot{\mathbf{r}}(s)\times\mathbf{n}(s)+\mathbf{l}(s)=0$. Typically, there are no body moments, so $\mathbf{l}(s)=0$, producing an overall moment balance of

$$\dot{\mathbf{m}}(s)+\dot{\mathbf{r}}(s)\times\mathbf{n}(s)=\mathbf{0}. \tag{5}$$

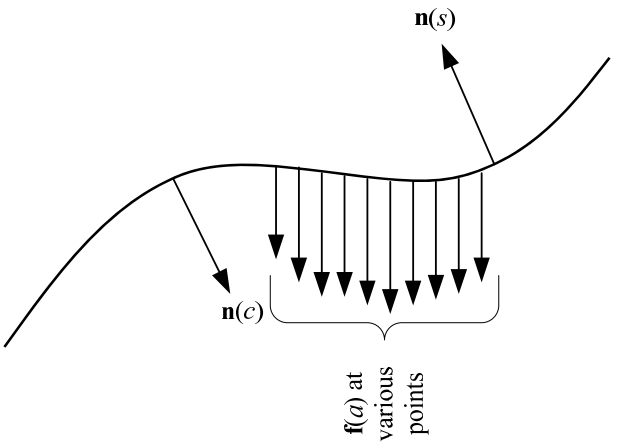

Fig. 3 The force balance considers a section of the rod from *c* to *s*, summing contact forces applied by that section to the remainder of the rod $\mathbf{n}(s)-\mathbf{n}(c)$ with body forces (such as gravity) $\int_c^s \mathbf{f}(\xi)\,d\xi$.

Next, the constitutive equations relate the force $\mathbf{n}^l=\begin{bmatrix} n_1^l & n_2^l & n_3^l \end{bmatrix}^{\mathrm{T}}$ the rod exerts along the local *x*, *y*, and *z* axes at a specific point *s*, termed the contact force, to the displacements $\mathbf{v}^l$ defined above. Likewise, constitutive equations also relate moments (torques) $\mathbf{m}^l=\begin{bmatrix} m_1^l & m_2^l & m_3^l \end{bmatrix}^{\mathrm{T}}$ to bending $\mathbf{u}^l$ about the local *x*, *y*, and *z* axes.

C. Constitutive equations

Constitutive equations define the deformation of a specific material resulting from an applied force or moment. Linear materials, such as many types of steel, obey Hooke's law $(F=k\Delta x)$. The nickel-titanium alloy Nitinol used for experimental validation in Section IV is Hookean at a constant temperature and low strain (< 1%), motivating a linear constitutive equation which relates the shear force $\mathbf{n}^l(s)$ applied by the rod at a specific point on the rod *s* to the change in shape $\mathbf{v}^l(s)$ at that point.

Because the rod extends along one axis $\mathbf{e}_e$ (in the 3-D case, the local z axis), $v_e^l = 1$ indicates the rest state (neither compressed nor stretched), whereas $v_i^l > 0$ indicates deformation for the other two axes. The constitutive equations are therefore

$$\mathbf{n}^l(s) = \mathbf{D}\left(\mathbf{v}^l(s) - \mathbf{e}_e\right) \tag{6}$$

where $\mathbf{D} = diag\left(\begin{bmatrix} D_1 & D_2 & D_3 \end{bmatrix}\right)$. Likewise, constitutive equations which relate moments $\mathbf{m}^l(s)$ in the local frame to local bending $\mathbf{u}^l(s)$ are

$$\mathbf{m}^l(s) = \mathbf{C}\mathbf{u}^l(s) \tag{7}$$

where $\mathbf{C} = diag\left(\begin{bmatrix} C_1 & C_2 & C_3 \end{bmatrix}\right)$. The C_k and D_k constants relate forces or moments to linear or angular displacements. Specifically, these constants are $C_1 = EI_1$, $C_2 = EI_2$, $C_3 = GJ$, $D_1 = D_2 = GA_T$, and $D_3 = EA_T$ where E specifies the modulus of elasticity, G the shear modulus, I the second moment of area, J the polar moment of inertia, and A_T the cross-sectional area of the rod.

D. Substitution and solution

First, the choice of gravity as body force defines $\mathbf{f}$ in (3)-(4); note that dependence on s from this point forward is dropped to present more compact equations. The mass per unit length of the rod at some point c depends both on the density $\rho(c)$ of the rod at that point and on the cross-sectional area $A(c)$ of the rod at c. Following convention, this is notated $(\rho A)(c)$. Given an acceleration due to gravity g and a unit vector $\mathbf{e}_g$ specifying its direction, gravity then exerts a force of $\mathbf{f}(a) = (\rho A)(a) g\mathbf{e}_g$ to a point a on the rod. When neither A nor ρ vary, this simplifies to $\mathbf{f}(a) = \rho A g\mathbf{e}_g$. Therefore, substituting this body force and (6) into (4), $\partial/\partial s\left(\mathbf{R}\mathbf{D}\left(\mathbf{v}^l - \mathbf{e}_e\right)\right) + \rho A g\mathbf{e}_g = \mathbf{0}$. Solving,

$$\dot{\mathbf{v}}^l = \mathbf{D}^{-1}\left(-\rho A g\mathbf{R}^{\mathrm{T}}\mathbf{e}_g - \hat{\mathbf{u}}^l\mathbf{D}\left(\mathbf{v}^l - \mathbf{e}_e\right)\right). \tag{8}$$

Likewise, substituting (7) and (1) into (5) gives $\partial/\partial s\left(\mathbf{R}\mathbf{C}\mathbf{u}^l\right) + \mathbf{R}\mathbf{v}^l \times \mathbf{D}\left(\mathbf{v}^l - \mathbf{e}_e\right) = \mathbf{0}$. Solving,

$$\dot{\mathbf{u}}^l = \mathbf{C}^{-1}\left(-\hat{\mathbf{u}}^l\mathbf{C}\mathbf{u}^l - \hat{\mathbf{v}}^l\mathbf{D}\left(\mathbf{v}^l - \mathbf{e}_e\right)\right). \tag{9}$$

Conveniently, use of (3) allows inclusion of a tip force $\mathbf{F}$, such as a mass located at the end of the robot, through the initial condition for $\mathbf{v}^l$. Choosing $s = s_f$ (where s_f specifies the unstretched length of the rod) and $c = 0$ (the beginning of the rod), the equation becomes $\mathbf{n}(0) = \mathbf{n}(s_f) + \int_0^{s_f}\mathbf{f}(\xi)d\xi$. Substituting (6) for $\mathbf{n}(0)$, choosing tip force $\mathbf{F} \equiv \mathbf{n}(s_f)$, recalling $\mathbf{f}(s) = \rho A g\mathbf{e}_g$, then solving,

$$\mathbf{v}^l(0) = \mathbf{D}^{-1}\mathbf{R}^{\mathrm{T}}(0)\left(\mathbf{F} + \rho A g s_f\mathbf{e}_g\right) + \mathbf{e}_e. \tag{10}$$

E. Evaluation using an ODE solver

Table I summarizes the equations derived in this section which are needed by an ODE solver. Any arbitrary initial conditions can be chosen for $\mathbf{r}$ and $\mathbf{R}$. Typically, the origin of the rod lies at the origin of the coordinate system, so that $\mathbf{r}(0) = \begin{bmatrix} 0 & 0 & 0 \end{bmatrix}^{\mathrm{T}}$. Likewise, $\mathbf{R}$ specifies the initial rod orientation. For example, if the rod is mounted so that it extends along the global x axis, then $\mathbf{R} = \begin{bmatrix} \mathbf{e}_2 & \mathbf{e}_3 & \mathbf{e}_1 \end{bmatrix}$ where $\mathbf{e}_i$ vectors represent vectors along the x, y, and z axes. In contrast, the initial bending $\mathbf{u}^l(0)$ must produce a moment applied to the trunk's tip, resulting in a boundary condition. From the constitutive equations, the tip moment $\mathbf{m}(s_f) = \mathbf{R}(s_f)\mathbf{C}\mathbf{u}^l(s_f)$. Therefore, after running the ODE, the error $\boldsymbol{\tau} - \mathbf{m}(s_f)$ where $\boldsymbol{\tau}$ specifies the applied tip moment allows a root-finding solver to guess a new $\mathbf{u}^l(0)$ initial value until the error between computed and applied tip moment is sufficiently small.

IV. Implementation and Experimental Validation

A rod composed of a nickel-titanium alloy termed Nitinol provides a good candidate for the backbone of a continuum robot, due to its ability to flex a large amount (up to 1% strain) without a permanent (plastic) deformation. However, its temperature-dependent modulus requires measurement of E and application at a constant temperature. A rod of diameter 1.56 mm, 40 cm in length, with a mass density of 6.80 g/cc as shown in Fig. 4 provided an experimental platform on which to validate the theory presented in this proposal. To determine the modulus of elasticity of the rod, the data (tip mass vs. deflection) was fit to the model, yielding E = 54 GPa. For a circular cross-section rod, $I = \pi d^4/64$ and $J = \pi d^4/32$ where d specifies the rod diameter. In this case, $I = 0.291$ pm^4 and $J = 0.581$ pm^4. Choosing Poisson's ratio $\nu = 0.3$, the shear modulus $G = E/(1+\nu) = 20.8$ GPa.

A. Experimental procedure

Fig. 4 shows the experimental setup, in which this rod was mounted horizontally on a sheet of acrylic with a laser-cut 1 mm grid. A friction-fit assembly located precisely with respect to the grid securely held the rod. A mass was attached to its tip with a string; 1 cm of the rod was used to fix the rod, leaving 39 cm of bending length. The measured position of the tip was compared to its predicted value; the distance between the two as a percentage of rod length gives the percent error. Table II summarizes the results, showing high accuracy in the model's predictions with an average tip position error of 2.1 mm (0.54% of the rod's length).

In contrast, analytical models define continuum robot shape as an arc of a circle tangent to the rod at its mounting

TABLE I
ODE SUMMARY

Initial condition	Meaning	Derivative to integrate
$\mathbf{r}(0)$	Location of trunk origin	$\dot{\mathbf{r}}$ from (1)
$\mathbf{R}(0)$	Initial trunk orientation	$\dot{\mathbf{R}}$ from (2)
$\mathbf{u}^l(0)$	Initial bending (found iteratively)	$\dot{\mathbf{u}}^l$ from (9)
$\mathbf{v}^l(0)$ from (10)	Initial stretch and shear	$\dot{\mathbf{v}}^l$ from (8)

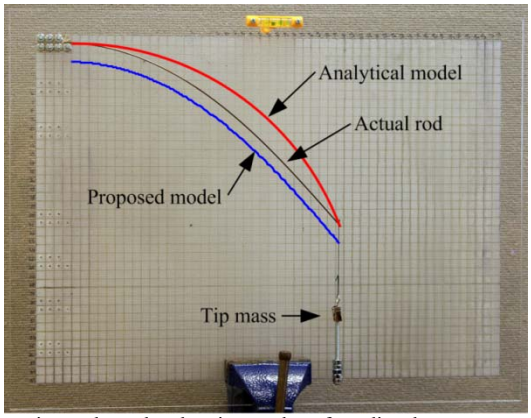

Fig. 4 Experimental results showing a plot of predicted versus actual rod shape using a model, which incorporates gravity versus one without gravity. The top line shows the analytical model which does not include gravity, while the bottom line shows the proposed model, offset vertically to make the physical rod visible.

point. To simplify the comparison, the endpoint of the analytical model was placed exactly on at the tip of the physical rod; even with this exact placement, this analytical model poorly fits the physical rod as shown in the figure.

V. Applications to Robotics

Several minor modifications to the theory presented thus far enable the use of these equations in the control of a continuum robot. Identifying an alternative to measuring tip torque significantly simplifies sensing the robot's position. The use of some basic real-time techniques, including a method which recasts the boundary-value problem into an initial-value problem, shows promise for real-time control. Finally, techniques to determine the Jacobian numerically allow for straightforward end-point control.

A. Alternatives to tip torque measurement

The solutions produced therefore determine a rod tip position **r** and orientation **R** based on a force **F** loading the tip (such as a tool located at the tip) and on a torque **τ** applied to the tip by actuators such as cables or pneumatic bellows. Although tip torque can be easily determined by measuring current driven to a DC motor or by attaching a load cell, mechanical considerations make this a less-desirable option. In particular, the loss inherent in most gear-reduction schemes necessary for motor operation reduces the accuracy of torque measurement or requires the adoption of low-loss transmissions such as cables or harmonic drives while the additional cost and complexity of a load cell make it a less-attractive alternative. In addition, the cable guides deliver some but not all force applied to the cables to the tip, with some forces lost as cables pass through the guides as discussed in [26], making it more difficult to accurately determine the tip torque based on cable force.

TABLE II
Experimental Results

	Predicted		Observed		Error	
Mass (g)	*x* (cm)	*y* (cm)	*x* (cm)	*y* (cm)	In mm	In %
0.00	38.93	-2.16	39.00	-2.30	1.5	0.39
13.80	34.87	-15.94	35.00	-15.90	1.4	0.35
16.90	33.64	-17.98	33.90	-17.80	3.2	0.82
20.00	32.43	-19.71	32.50	-19.50	2.2	0.55
23.10	31.28	-21.16	31.40	-21.20	1.2	0.31
26.20	30.20	-22.40	30.30	-22.40	1.0	0.26
29.30	29.18	-23.47	29.50	-23.30	3.6	0.92
32.40	28.24	-24.38	28.50	-24.40	2.6	0.68
35.50	27.35	-25.17	27.40	-25.40	2.3	0.58
38.60	26.53	-25.86	26.50	-26.20	3.3	0.85
41.70	25.77	-26.48	25.80	-26.90	4.2	1..07
				Average	2.4	0.61

The (x, y) locations give predicted versus measured tip positions. Percent error = error / rod length.

In the case of a cable-actuated robot, it is therefore often simpler to determine cable length (using, for example, inexpensive and widely-available encoders) than force applied to the cables which produces the torque **τ**. The necessary cable lengths can be easily determined based on the intermediate points $\mathbf{r}(0\ldots s_f)$ and $\mathbf{R}(0\ldots s_f)$ produced by the ODE solver, a vector $\mathbf{l}^j$ from the rod center to the cable guides, and the location $s_{1\ldots n}$ of the n cable guides along the rod. Specifically, noting that the homogenous transformation matrix $\mathbf{T}_i = \begin{bmatrix} \mathbf{R}(s_i) & \mathbf{r}(s_i) \\ \mathbf{0} & 1 \end{bmatrix}$ maps from local coordinates of cable guide i to global coordinates and that that the location of the cable guides is at $\mathbf{l}^j$ in the local coordinate frame, then the location of the cable guide in the global coordinate frame is $\bar{\mathbf{l}} = \mathbf{T}\bar{\mathbf{l}}^j$, where the over bar indicates use of homogenous coordinates. Summing the distances between each guide determines the overall cable length, which produces the calculated rod shape:

$$l_j = \sum_{i=2}^{n-1} \left\| \mathbf{T}_i \bar{\mathbf{l}}_j^j - \mathbf{T}_{i-1} \bar{\mathbf{l}}_j^j \right\|_2 \tag{11}$$

where l_j represents the length of the j^{th} cable.

B. Jacobian calculation and application

While the Jacobian for rigid-link robots can be derived analytically by computing the relevant derivative (or by standard schemes which obviate the need for computing these derivates [27, 28]), these derivates cannot be likewise computed for rod statics, because the rod tip position and orientation do not depend directly on the tip force or moment. However, a numerical approach suffices to determine the derivatives.

This Jacobian will be computed based on $\mathbf{u}^l(0)$ rather than **τ**, improving computational efficiency while also avoiding discontinuities arising from multiple solutions which exist for the boundary-value problem. For notational convenience, define $\mathbf{r}(s_f)$ calculated with initial conditions of **F** and $\mathbf{u}^l(0)$ to be $\mathbf{r}_f(\mathbf{F}, \mathbf{u}_0^l)$. The Jacobian is then

$$\mathbf{J} = \delta^{-1}\left[\mathbf{r}_f\left(\mathbf{F} + \delta\mathbf{e}_{1\ldots3}, \mathbf{u}_0^l\right) - \mathbf{r}_f\left(\mathbf{F}, \mathbf{u}_0^l\right) \quad \mathbf{r}_f\left(\mathbf{F}, \mathbf{u}_0^l + \delta\mathbf{e}_{1\ldots3}\right) - \mathbf{r}_f\left(\mathbf{F}, \mathbf{u}_0^l\right)\right]$$

where $\mathbf{r}_f\left(\mathbf{F} + \delta\mathbf{e}_{1\ldots3}, \mathbf{u}_0^l\right)$ serves as shorthand for three evaluations of $\mathbf{r}_f\left(\mathbf{F}, \mathbf{u}_0^l\right)$ and δ provides a small value over which the Jacobian is assumed to be nearly linear. An analogous procedure allows computation of angular velocity, with the

added complexity of transforming the resulting matrix derivates $\dot{\mathbf{R}}$ into angular velocity vectors $\hat{\boldsymbol{\omega}} = \dot{\mathbf{R}}\mathbf{R}^{\mathrm{T}}$.

C. Real-time considerations

Real-time computation of the statics derived above is essential when operating a continuum robot. Several simple approaches enable computation of the statics for a single-section trunk in 3-D (equivalent to forward kinematics for rigid-link robots) at ~125 Hz on a 2.60 GHz AMD Athlon x64 dual-core CPU. First, solution of an initial-value problem rather than the boundary-value problem and its associated iterative root-finding significantly lowers the computations burden. Due to the procedure outlined above, only cable length, not tip torque, is necessary to shape the robot. Therefore, initial values for $\mathbf{u}^{l}$ can be used when determining the statics solution. Second, lowering the error tolerance of the ODE solver speeds computation. Specifically, choosing a relative error tolerance of $1 \cdot 10^{-3}$ and an absolute error tolerance of $1 \cdot 10^{-6}$ provides accuracy which meets or exceeds the accuracy of which the trunk is capable while also providing good real-time performance. This speed could be improved by implementing the code in a compiled language; all performance results reported rely on m-file programs executing in MATLAB.

VI. Conclusion

In conclusion, this paper presents an accurate 3-D statics model for a continuum robot based on Cosserat rod theory, which incorporates the significant effects of gravity loading on the resulting shape of the rod. The model demonstrates excellent accuracy with an error of 0.61% in the predicted versus measured tip position when compared with a physical rod, providing initial validation of the technique. Real-time performance of 125 Hz makes this approach a viable candidate for control of a continuum robot. Future work includes the use of this model in the control of a prototype continuum robot as shown in Fig. 1.

References

[1] W. M. Kier and K. K. Smith, "Tongues, tentacles and trunks: the biomechanics of movement in muscular-hydrostats," *Zoological Journal of the Linnean Society,* vol. 83, pp. 307-324, 1985.

[2] K. Salisbury, W. Townsend, B. Ebrman, and D. DiPietro, "Preliminary design of a whole-arm manipulation system (WAMS)," in *Proceedings of the IEEE International Conference on Robotics and Automation*, Philadelphia, Pennsylvania, 1988, pp. 254-260.

[3] B. A. Jones, M. Csencsits, W. McMahan, V. Chitrakaran, M. Grissom, M. Pritts, C. D. Rahn, and I. D. Walker, "Grasping, manipulation, and exploration tasks with the OctArm continuum manipulator," in *video in Proceedings of the International Conference on Robotics and Automation*, Orlando, FL, USA, 2006.

[4] S. Neppalli, B. A. Jones, M. Csencsits, W. McMahan, V. Chitrakaran, M. Grissom, M. Pritts, C. D. Rahn, and I. D. Walker, "OctArm - Soft Robotic Manipulator," in *video in Proceedings of the International Conference on Intelligent Robots and Systems* San Diego, CA, USA, 2007.

[5] W. McMahan, B. A. Jones, I. D. Walker, V. Chitrakaran, A. Seshadri, and D. Dawson, "Robotic manipulators inspired by cephalopod limbs," in *Proc. of the CDEN Design Conf.*, Montreal, Canada, 2004, pp. 1-10.

[6] P. Sears and P. Dupont, "A Steerable Needle Technology Using Curved Concentric Tubes," in *Proceedings of the IEEE/RSJ International Conference on Intelligent Robots and Systems*, Beijing, China, 2006, pp. 2850-2856.

[7] R. J. Webster, A. M. Okamura, and N. J. Cowan, "Toward Active Cannulas: Miniature Snake-Like Surgical Robots," in *IEEE/RSJ International Conference on Intelligent Robots and Systems*, Beijing, China, 2006, pp. 2857-2863.

[8] Y. Bailly and Y. Amirat, "Modeling and Control of a Hybrid Continuum Active Catheter for Aortic Aneurysm Treatment," in *Proceedings of the IEEE International Conference on Robotics and Automation*, Barcelona, Spain, 2005, pp. 936-941.

[9] G. Chen, M. T. Pham, and T. Redarce, "Development and kinematic analysis of a silicone-rubber bending tip for colonoscopy," in *Proceedings of the IEEE/RSJ International Conference on Intelligent Robots and Systems*, Beijing, China, 2006, pp. 168-173.

[10] N. Simaan, "Snake-Like Units Using Flexible Backbones and Actuation Redundancy for Enhanced Miniaturization," in *Proceedings of the IEEE International Conference on Robotics and Automation*, Barcelona, Spain, 2005, pp. 3023-3028.

[11] G. Immega, K. Antonelli, and J. Ko, "Teleoperation of the KSI Tentacle Manipulator for hot cell decontamination," in *Proceedings of the IEEE International Conference on Intelligent Systems for the 21st Century*, Vancouver, Canada, 1995, pp. 2133-2136.

[12] OC Robotics, "Snake-arm robots access the inaccessible," *Nuclear Technology International,* vol. 1, pp. 92-94, 2008.

[13] V. C. Anderson and R. C. Horn, "Tensor arm manipulator design," *Transactions of the ASME,* vol. 67-DE-57, pp. 1–12, 1967.

[14] D. M. Lane, J. B. C. Davies, G. Robinson, D. J. O'Brien, J. Sneddon, E. Seaton, and A. Elfstrom, "The AMADEUS dextrous subsea hand: design, modeling, and sensor processing," *IEEE Journal of Oceanic Engineering,* vol. 24, pp. 96-111, Jan. 1999.

[15] H. Tsukagoshi, A. Kitagawa, and M. Segawa, "Active Hose: an artificial elephant's nose with maneuverability for rescue operation," in *Proceedings of the IEEE International Conference on Robotics and Automation*, Seoul, Korea, 2001, pp. 2454-2459.

[16] G. Robinson and J. B. C. Davies, "Continuum robots - a state of the art," in *Proceedings of the IEEE International Conference on Robotics and Automation*, Detroit, Michigan, 1999, pp. 2849-2854.

[17] D. Trivedi, A. Lotfi, and C. D. Rahn, "Geometrically exact dynamic models for soft robotic manipulators," in *IEEE/RSJ International Conference on Intelligent Robots and Systems*, San Diego, CA, 2007, pp. 1497-1502.

[18] M. W. Hannan and I. D. Walker, "Kinematics and the Implementation of an elephant's trunk manipulator and other continuum style robots," *Journal of Robotic Systems,* vol. 20, pp. 45-63, Feb. 2003.

[19] B. A. Jones and I. D. Walker, "Kinematics for Multisection Continuum Robots," *IEEE Transactions on Robotics,* vol. 22, pp. 43-55, Feb. 2006.

[20] S. Neppalli and B. A. Jones, "Design, Construction, and Analysis of a Continuum Robot," in *Proceedings of the International Conference on Intelligent Robots and Systems*, San Diego, CA, USA, 2007, pp. 1503-1507.

[21] S. Hirose, *Biologically inspired robots*. New York, NY: Oxford University Press, 1993.

[22] G. S. Chirikjian and J. W. Burdick, "A modal approach to hyper-redundant manipulator kinematics," *IEEE Transactions on Robotics and Automation,* vol. 10, pp. 343-354, June 1994.

[23] S. S. Antman, *Nonlinear problems of elasticity*, 2nd ed. New York: Springer, 2005.

[24] M. Ivanescu, M. C. Florescu, N. Popescu, and D. A. P. D. Popescu, "Coil function control problem for a hyperredundant robot," in *IEEE/ASME International Conference on Advanced Intelliget Mechatronics*, Zurich, Switzerland, 2007, pp. 1-6.

[25] I. A. Gravagne, C. D. Rahn, and I. D. Walker, "Large deflection dynamics and control for planar continuum robots," *IEEE/ASME Transactions on Mechatronics,* vol. 8, pp. 299-307, June 2003.

[26] I. Gravagne, "Design, Analysis and Experimentation: The Fundaments of Continuum Robotic Manipulators," in *Department of Electrical Engineering*. vol. Ph.D. Clemson: Clemson University, 2002.

[27] M. W. Spong, S. Hutchinson, and M. Vidyasagar, *Robot modeling and control*. New York: John Wiley & Sons, Inc., 2006.

[28] J. J. Craig, *Introduction to robotics: mechanics and control*, 3rd ed. Upper Saddle River, NJ: Pearson Prentice Hall, 2005.